

# Pseudo-magnetoexcitons in strained graphene bilayers without external magnetic fields

Zhigang Wang,<sup>1</sup> Zhen-Guo Fu,<sup>2,1</sup> Fawei Zheng,<sup>1</sup> and Ping Zhang<sup>1,3</sup>

<sup>1</sup>*LCP, Institute of Applied Physics and Computational Mathematics,  
P. O. Box 8009, Beijing 100088, China*

<sup>2</sup>*SKLSM, Institute of Semiconductors, CAS,  
P. O. Box 912, Beijing 100083, China*

<sup>3</sup>*Beijing Computational Science Research Center, Beijing 100089, China*

## Abstract

The structural and electronic properties of graphene leads its charge carriers to behave like relativistic particles, which is described by a Dirac-like Hamiltonian. Since graphene is a monolayer of carbon atoms, the strain due to elastic deformations will give rise to so-called ‘pseudomagnetic fields (PMF)’ in graphene sheet, and that has been realized experimentally in strained graphene sample. Here we propose a realistic strained graphene bilayer (SGB) device to detect the pseudo-magnetoexcitons (PME) in the absence of external magnetic field. The carriers in each graphene layer suffer different strong PMFs due to strain engineering, which give rise to Landau quantization. The pseudo-Landau levels (PLLs) of electron-hole pair under inhomogeneous PMFs in SGB are analytically obtained in the absence of Coulomb interactions. Based on the general analytical optical absorption selection rule for PME, we show that the optical absorption spectrums can interpret the corresponding formation of Dirac-type PME. We also predict that in the presence of inhomogeneous PMFs, the superfluidity-normal phase transition temperature of PME is greater than that under homogeneous PMFs.

Graphene has been an optimal playground to realize the exciting ideas in condensed matter physics [1–3] since the carriers in graphene behave like massless Dirac particles. Many efforts have been devoted to detecting the striking electronic properties of graphene, such as Klein paradox [4], anomalous quantum Hall effect [5], and so on. However, it was soon realized that the structural and mechanical properties should also be important both from theoretical interest and from applications of graphene [6], such as the strain engineering in graphene [7–14]. It has been shown recently that specific forms of strain produce a strong PMF in graphene, which effectively break the time-reversal symmetry [9]. The strain-induced PMF is expected to produce PLLs, and consequently, the quantum Hall effect, even in the absence of external magnetic field [10]. These intriguing properties extend to graphene multilayers. Recently, the shear mode in graphene multilayers has been observed in Raman spectroscopy experiment [15], and the high temperature Bose-Einstein condensation and superfluidity of indirect excitons or electron-hole pairs in Graphene  $n$ - $p$  bilayers [16–19] are also predicted. Differing from other bilayer  $n$ - $p$  systems, such as coupled semiconductor quantum wells [20–22],  $n$ - $p$  type SGB separated by a dielectric layer should be an ideal setup to create PME due to the PMF induced by strain rather than the applied magnetic field. Because of the difference of ripples or elastic deformations in each graphene layer sample on a substrate, in fact, it is more realistic to fabricate different or say inhomogeneous PMFs in electron and hole layers, which is hard to realize with external magnetic fields.

On the basis of these interesting and reasonable ideas, in the present work, we will theoretically analyze the PME properties in SGB device without applying magnetic field. In the following, we show that the formation of PME in SGB could be determined from the optical absorption selection rule of PME, which is related to the imbalance parameter  $\gamma = \sqrt{B_s^h/B_s^e}$  of the strain-induced PMFs  $B_s^h$  and  $B_s^e$  suffered by Dirac holes and electrons in SGB. We also find that comparing with homogeneous case ( $\gamma=1$ ), the Kosterlitz-Thouless (KT) transition critical temperature will be improved by a factor of  $[(2+\gamma+\gamma^{-1})/4]^2$ . Moreover, we suggest some technical skills for designing the SGB setup that can make use of this realization to detect PME.

As illustrated in Fig. 1, the system we considered here is that of two parallel strained graphene layers separated by an insulating slab of  $\text{SiO}_2$ . By varying the chemical potential via tuning the bias voltages of the two gates located near the corresponding graphene sheets,

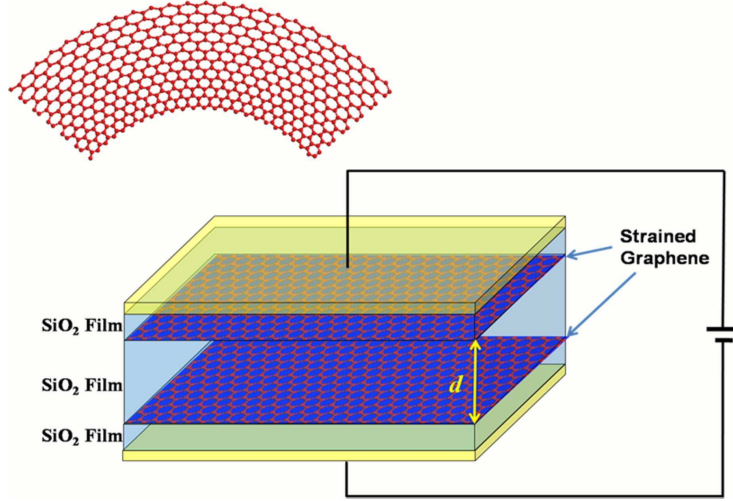


FIG. 1: (Color online) **Basic Scheme of the proposed SGB device.** Two strained graphene monolayers are separated by dielectric spacer. Electron/hole carriers in each layer are created by  $n(p)$ -type doping or applied external gates. Indirect PME can be generated by PMFs in SBG. Uniform PMF perpendicular to the graphene surface is created in a circular arc strained graphene ribbon.

the spatially separated electrons and holes in different layers can be generated. In order to obtain the analytical PLL expression, we suppose both graphene sheets are bent to circular arc [11], which can lead to PMFs  $B_s^{e/h} = 8\beta c^{e/h}/a_0$  (in unit of  $\hbar/e \equiv 1$ ), and the corresponding fictitious gauge field vector potentials can be chosen as  $\mathbf{A}_s^{e/h} = B_s^{e/h} (0, x^{e/h})$ . Here,  $a_0$  is the lattice constant,  $\beta = -\partial \ln t / \partial \ln a_0 \approx 2$  and  $t$  denotes the nearest-neighbor hopping parameter, and  $c^{e/h}$  is the numerical constant representing the strength of strain in electron/hole layers. In general  $c^e \neq c^h$ , and thus  $B_s^e \neq B_s^h$  in SGB device, which results in the fact that  $\gamma$  departs from 1.

This SGB system is described by the Hamiltonian  $H = H_0 + U(\mathbf{r}^e - \mathbf{r}^h)$ , where

$$H_0 = \hbar v_f [\pi_x^e \sigma_1 \otimes \sigma_0 - \pi_y^e \sigma_2 \otimes \sigma_0 + \pi_x^h \sigma_0 \otimes \sigma_1 - \pi_y^h \sigma_0 \otimes \sigma_2], \quad (1)$$

with Fermi velocity  $v_f \approx 10^6 \text{ m} \cdot \text{s}^{-1}$ ,  $\pi^{e/h} = \mathbf{p}^{e/h} \mp \frac{e}{c} \mathbf{A}_s^{e/h}$ , and Pauli matrices  $\sigma_i$  ( $i=0, 1, 2$ ).  $U(\mathbf{r}^e - \mathbf{r}^h) = -e^2 / \epsilon \sqrt{|\mathbf{r}^e - \mathbf{r}^h|^2 + d^2}$  is Coulomb interaction (CI) between the pair of spatially separated electron and hole, where  $d$  is the spacer thickness and  $\epsilon$  ( $\sim 4.5$  for  $\text{SiO}_2$ ) denotes the dielectric constant of spacer. In the following text, the relative CI strength notation is taken as  $\lambda \equiv (e^2 / \epsilon) / (\hbar v_f)$ . Taking some coordinate transformations, the free part of Hamiltonian

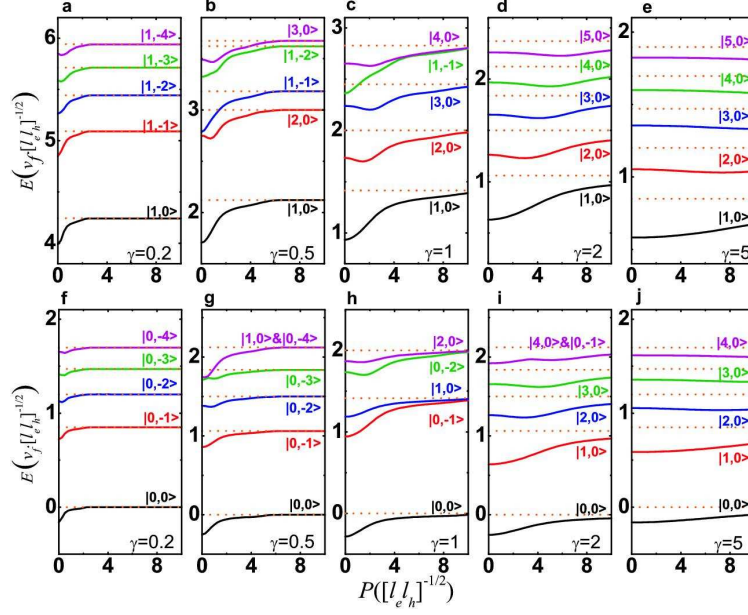


FIG. 2: (Color online) **Dispersions of the first few PLLs for fully occupied case (upper panels) and partially occupied (lower panels) case, as functions of  $P$  with different  $\gamma$ .** The dashed horizontal lines denote the non-interacting PLLs. The parameters are chosen as  $\mu=0$ ,  $\lambda=0.49$ ,  $d=0.2$ , and  $R=0$ .

$H$  can be written as

$$H_0 = \frac{\hbar v_f (l_e + l_h)}{\sqrt{2} (l_e l_h)^{3/2}} \begin{pmatrix} 0 & l_h c_+ & l_e c_-^\dagger & 0 \\ l_h c_+^\dagger & 0 & 0 & l_e c_-^\dagger \\ l_e c_- & 0 & 0 & l_h c_+ \\ 0 & l_e c_- & l_h c_+^\dagger & 0 \end{pmatrix}, \quad (2)$$

with  $l_{e/h} = \sqrt{\hbar/eB_s^{e/h}}$  the pseudomagnetic lengths in electron/hole layer (in following text, we set the length unit as  $\sqrt{l_e l_h}$ ) and the harmonic lowering operators  $c_\pm$  (see Supplementary Information part I).

To obtain eigenvalues  $E_{n_+, n_-}$  of the total Hamiltonian  $H$ , the CI part  $U$  needs to be treated as a perturbation in the first order  ${}_0\langle n'_+, n'_- | U | n_+, n_- \rangle_0$ , where  $|n_+, n_- \rangle_0$  is the eigenstates of  $H_0$  corresponding to the eigenvalues, i.e., the PLLs of  $H_0$  without CI

$$E_{n_+, n_-}^{(0)} = \frac{1}{\sqrt{2}} \left[ s_+ \sqrt{|n_+|} (1 + \gamma^{-1}) - s_- \sqrt{|n_-|} (1 + \gamma) \right] \quad (3)$$

in units of  $\hbar v_f / \sqrt{l_e l_h}$ , with  $s_\pm = \text{sgn}(n_\pm)$ . The imbalance parameter  $\gamma$  will reduce the degen-

eracy of PLLs of  $H_0$ . For instance,  $|1, 0\rangle_0$  and  $|0, -1\rangle_0$  are degenerate when  $\gamma=1$ , while these two states turn to be nondegenerate when  $\gamma \neq 1$ . The PLLs  $E_{n_+, n_-}$  of PME are not only dependent on  $\gamma$ , but also related to the effective momentum  $\mathbf{P} = 2\frac{l_e \mathbf{p}^e + l_h \mathbf{p}^h}{l_e + l_h}$  and coordinate  $\mathbf{R} = \frac{l_h \mathbf{r}^e + l_e \mathbf{r}^h}{l_e + l_h}$  of the mass center of PME since  $U$  is related to  $\mathbf{P}$  and  $\mathbf{R}$  after transformations (see Supplementary Information part I). The location of the chemical potential will determine the attainable possible PLL indices for electrons and holes. For convenience, in this work we choose the notation  $\mu$  describing the highest filled PLL and consider two cases: (i) the electron-PLLs with  $n_+ > \mu$  are unoccupied and the hole-PLLs with  $n_- \leq \mu$  are fully occupied; and (ii) the electron-PLLs with  $n_+ > \mu$  are unoccupied and the hole-PLLs with  $n_- < \mu$  are fully occupied, while the PLL at  $\mu$  is partially occupied.

The spectrums of the lowest five PLLs as a function of  $\mathbf{P}$  are demonstrated in Fig. 2. Figures 2a–2e correspond to the fully occupied cases while Figs. 2f–2j are for the partially occupied cases. The PME dispersion strongly depends on the imbalance parameter  $\gamma$  (see Fig. 2). On one hand, if the difference in the elastic deformations between electron and hole layers is large, i.e.,  $\gamma$  departs from  $\gamma=1$  greatly, the PME dispersion will accelerate the transition process from density wave forms to particle-hole pair forms with increasing the momentum  $\mathbf{P}$ . On the other hand, when  $\gamma$  takes a moderate value around 1, the PME dispersion behaves like that of magnetoexcitons in perfect graphene bilayers under an external magnetic field. Besides, we also found that, taking the partially occupied cases as an example, at much larger  $\gamma$  the lowest PLLs behave like electron type  $|n_+, 0\rangle$  (for example, Fig. 2j) while at much smaller  $\gamma$  the lowest PLLs behave like hole type  $|0, n_- \rangle$  (for example, Fig. 2f). Differing from the magnetoexcitons in an external magnetic field, the PME dispersion is also related on  $\mathbf{R}$ . By increasing  $R$ , the PME dispersion at smaller  $P$  turns to become a particle-hole pair form rather than a density-wave form (Supplementary Figure S1).

The optical absorption spectroscopy analysis is an instructive method in studying the properties of magnetoexcitons, because it can determine the knowledge of magnetoexciton's energies and wave functions at  $\mathbf{P}=0$ . The particle-hole excitation energy should be revealed directly by the resonant peaks in the magneto-optical absorption spectroscopy  $R_{ab}(R, \omega) \propto \sum_{n_+, n_-} |\langle n_+, n_- | v_x | \mu, \mu \rangle|^2$ . In the absence of inter-PLL CI which is much weaker than intra-PLL CI, for linear polarized light  $\mathbf{A} = A\hat{\mathbf{x}}$ , the optical absorption selection rule

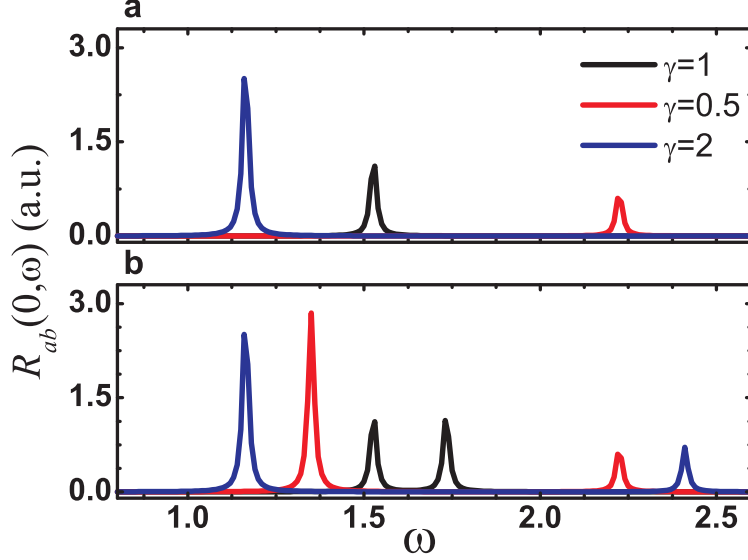


FIG. 3: (Color online) **The optical absorption curves of PME with  $\mu=0$ .** **a**, Fully and **b** partially occupied cases as functions of photon energy  $\omega$  ( $\hbar=1$ ). The spacer thickness is set to  $d=0.2$ .  $\lambda=0.49$ .

for PME is analytically expressed as

$$\begin{aligned} \langle n_+, n_- | v_x | \mu, \mu \rangle = & c_1 \delta_{|n_+, |\mu|} \delta_{|n_-, |\mu|-1} + c_2 \delta_{|n_+, |\mu|-1} \delta_{|n_-, |\mu|} \\ & + c_3 \delta_{|n_+, |\mu|} \delta_{|n_-, |\mu|+1} + c_4 \delta_{|n_+, |\mu|+1} \delta_{|n_-, |\mu|}, \end{aligned} \quad (4)$$

where  $v_x = \partial H_0 / \hbar \partial p_x$  is the velocity operator for free part of Hamiltonian, and the coefficients  $c_1 = -(1+\gamma)s_-(s_\mu s_+ + 1)C$ ,  $c_2 = (1+\gamma^{-1})(s_\mu + s_-)C$ ,  $c_3 = -(1+\gamma)(s_\mu + s_+)C$ , and  $c_4 = (1+\gamma^{-1})s_+(s_\mu s_- + 1)C$  with  $C = v_f(\sqrt{2})^{\delta_{n_+, 0} + \delta_{n_-, 0} + 2\delta_{\mu, 0} - 6}$  (see Supplementary Information part II). This optical absorption selection rule formula (4) offers a better way to analyze PME absorption resonant peaks in spectroscopy of SGB device. Notice that the optical absorption formula (4) also depends on  $\mathbf{R}$  since the PME spectrum is related to  $\mathbf{R}$ . (For brevity, we just consider the  $R=0$  case in following text.)

Especially, for the fully occupied case with  $\mu \geq 0$ , the selection rule can be further simplified as

$$\langle n_+, n_- | v_x | \mu, \mu \rangle = c_4 \delta_{n_+, \mu+1} \delta_{n_-, \mu}, \quad (5)$$

which indicates that there is only one resonance peak occurring in optical absorption spectrum, which corresponds to the formation of PME. For example, the selection rule for fully

occupied case of  $\mu=0$  with the ground state  $|0,0\rangle$  promises that just one resonance peak that corresponds to the formation of PME state  $|1,0\rangle$  occurs, see Fig. 3a. From Fig. 3a one can also clearly observe that with the imbalance parameter  $\gamma$  decreasing (increasing) from 1, the resonance peak moves towards high (low) frequency region, see the red (blue) curve in Fig. 3a.

This effect of inhomogeneity of PMFs can also be seen for the partially occupied cases, which is illustrated in Fig. 3b. According to the general selection rule (4), the nonzero elements of  $\langle n_+, n_- | v_x | 0, 0 \rangle$  only occurs at two PMEs states  $|1, 0\rangle$  and  $|0, -1\rangle$ , and thus in this case, there are two resonance peaks occurring in Fig. 3b. Interestingly, with decreasing (increasing)  $\gamma$  from 1, the resonance peak of  $|0, -1\rangle$  moves towards low (high) frequency region, in contrast, the resonance peak of  $|1, 0\rangle$  moves towards high (low) frequency region. The results of cases with  $\mu \neq 0$  are similar to these of  $\mu=0$ , and an example for  $\mu=1$  is shown in Supplementary Figure S2.

At this stage, we have not considered the effect of the inter-PLL CIs on the optical absorption of the PMEs. Because the inter-PLL CI mixes the noninteracting PLLs, the absorption phenomenon should appear at the energy of every PME states. Consequently, additional resonance peaks, except of the main peaks without the inter-PLL CI, will appear in the optical absorption spectrum (not shown here). The magnitudes of these additional resonant peaks are very tiny and tend to disappear by increasing the spacer thickness  $d$ . Therefore, based on the optical absorption selection rule analyzed above, one can see that the optical techniques should allow detection of PME locally as well as the CI effects in the present SGB device.

PMEs are also ideal objects in exploring the Bose-Einstein condensation since they behave as neutral bosons at low densities. Motivated by its importance both from basic point of interest and from application of graphene-based electronics, now we turn to address this issue by presenting an attempt at the theoretical evaluation of effective mass the effective mass  $m_{B_s}$  ( $B_s \equiv \sqrt{B_s^e B_s^h}$  herein) and superfluid-normal state, i.e., KT transition temperature  $T_c$  of PME in this SGB system. As an example, let us now consider the case of PME on the  $(1, 1)$ -PLL, with the PME energy at small magnetic momenta  $E_{1,1}(P) = \varepsilon_{B_s}^{(b)}(d) + \frac{P^2}{2m_{B_s}(d)}$  (see Supplementary Information part III and ref. 26). In the special limit of  $d \gg \sqrt{l_e l_h}$ , one can explicitly obtain  $\varepsilon_{B_s}^{(b)} = -\frac{e^2}{\epsilon d}$ , which is same as that of magnetoexcitons in external magnetic

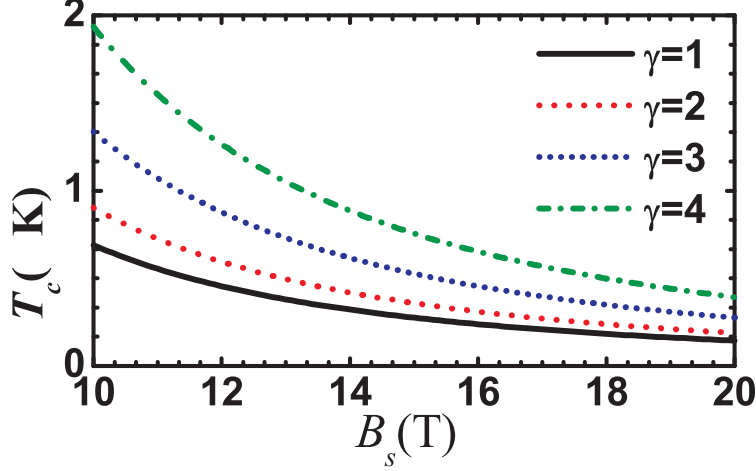


FIG. 4: (Color online) **Calculated KT temperature versus the PMF.** The density of PME is set as  $n=4.0 \times 10^{11} \text{cm}^{-2}$  and the spacer width  $d=30 \text{ nm}$ .

field since  $\varepsilon_{B_s}^{(b)}(d)$  is independent of  $\gamma$ . Whereas the effective mass of PME should be

$$m_{B_s} = [4 / (2 + \gamma + \gamma^{-1})]^2 \frac{\epsilon}{4c^2} d^3 B_s^2, \quad (6)$$

where the prefactor  $[4 / (2 + \gamma + \gamma^{-1})]^2$  will reduce to unity in the case of homogeneous PMFs (i.e.,  $\gamma=1$ ), thus that the effective mass of PME in SGB is  $[4 / (2 + \gamma + \gamma^{-1})]^2$  times of that of magnetoexcitons in perfect bilayer graphene under an external magnetic field. It is this difference between the effective masses that results in the difference in the KT transition temperature  $T_c$ , which reads

$$T_c = \left[ \left( \sqrt{\frac{32}{27} [(sm_{B_s} k_B T_c^0) / (\pi \hbar^2 n)]^3 + 1} + 1 \right)^{1/3} - \left( \sqrt{\frac{32}{27} [(sm_{B_s} k_B T_c^0) / (\pi \hbar^2 n)]^3 + 1} - 1 \right)^{1/3} \right] \frac{T_c^0}{2^{1/3}}, \quad (7)$$

where the auxiliary quantity is  $T_c^0 = \frac{1}{k_B} \left( \frac{\pi \hbar^2 n \mu_0^2}{6s\zeta(3)m_{B_s}} \right)^{1/3}$  with  $\mu_0 = \frac{\pi \hbar^2 n}{sm_{B_s} \log[s \hbar^4 \epsilon^2 / (2\pi n m_{B_s}^2 e^4 d^4)]}$  being the chemical potential of system,  $s=4$  the spin degeneracy of PMEs in SGB, and  $\zeta(3)$  the Riemann zeta function. Here,  $n = n_s + n_n$  with  $n_n$  the normal component density, and  $n_s$  the superfluid density. Because  $\mu_0$  approximately inverse of the effective mass, a rough consequence can be immediately obtained that the critical temperature of KT transition of PME in SGB will be greater  $[(2 + \gamma + \gamma^{-1}) / 4]^2$  times than that of magnetoexciton in bilayer



graphene in an external magnetic field [18]. Typical results are exhibited in Fig. 4. Thereby, one can conclude that increasing the imbalance of the strains ( $\gamma$  departs from 1 sufficiently) in different layers in SGB device may be one effective method to promote the KT transition temperature of PME.

In order to design the required SGB device in experiment, firstly, one should deposit graphene ribbons onto a elastic substrate and then deform it by bending it into a circular arc automatically (Fig. 1). Following that, we can transfer it onto the  $\text{SiO}_2$  thin film and then throw off the elastic substrate by heating or dissolving it via chemical agent carefully. A uniform PMF could be created in graphene ribbons deposited on  $\text{SiO}_2$  thin film since the strain distribution in the substrate would project onto graphene ribbon. In reality, the PMFs arisen from strain in upper and lower bent graphene ribbons, however, may be different because of different automatic deformations of them. This is why we discuss the importance of the imbalance parameter  $\gamma$  here. After that one can grow or evaporate metal electrode on the other side of  $\text{SiO}_2$  thin film, and finally package the device for measurements. The experimental capability to produce high quality graphene sample and the feasibility to create strong PMF in graphene, together with the technical advances for designing graphene multi-layer devices make it possible to perform very original optical and superfluidity-normal states KT transition experiments of PME in graphene without external magnetic field. Moreover, the SGB device proposed here could also be used to detect the (valley polarized) unconventional fractional quantum Hall effect of charged Dirac-type electron-hole fluid or a Bose condensate of PME in the absence of external magnetic field by measuring transport coefficients and that, since fixed PME number corresponds to fixed valley polarization in the SGB device, transport studies of the SGB system will provide unique information which cannot be observed by direct study of conventional two-component electron-electron/electron-hole systems [22, 23].

In summary, in this work we propose a realistic SGB device, and based on the physics analyzed here, this setup can be made to detect the PME which is associated with the elastic deformations or curvature in graphene. The cases discussed in this paper are only illustrative examples of the feasible setup and applications of the SGB device, and the technical skills mentioned above are achievable in current experimental capabilities. Therefore, we hope

these predictions and the suggested SGB device can be realized sooner rather than later.

---

- [1] Novoselov K. S., Geim A. Morozov K., S. V., Jiang D., Zhang Y., Dubonos S. V., Grigorieva I. V. & Firsov A. A. Electric Field Effect in Atomically Thin Carbon Films. *Science* **306**, 666-669 (2004).
- [2] Castro Neto A. H., Guinea F., Peres N. M. R., Novoselov K. S., & Geim A. K. The electronic properties of graphene. *Rev. Mod. Phys.* **81**, 109 (2009) and references therein.
- [3] Goerbig M. O. Electronic properties of graphene in a strong magnetic field. *Rev. Mod. Phys.* **83**, 1193 (2011) and references therein.
- [4] Katsnelson M. I. , Novoselov K. S. & Geim A. K. Chiral tunnelling and the Klein Paradox in graphene. *Nature Phys.* **2**, 620-625 (2006).
- [5] Zhang Y., Tan Y.-W., Stormer H. L. & Kim P. Experimental observation of the quantum Hall effect and Berry's phase in graphene. *Nature* **438**, 201-204 (2005).
- [6] Geim A. K. & Novoselov K. S. The rise of graphene. *Nature Mater.* **6**, 183-191 (2007).
- [7] Pereira V. M. & Castro Neto A. H. Strain Engineering of Graphene's Electronic Structure. *Phys. Rev. Lett.* **103**, 046801 (2009).
- [8] Levy N., Burke S. A., Meaker K. L., Panlasigui M., Zettl A., Guinea F., Castro Neto A. H. & Crommie M. F. Strain-Induced Pseudo-Magnetic Fields Greater Than 300 Tesla in Graphene Nanobubbles. *Science* **329**, 544-547 (2010).
- [9] Vozmediano M., Katsnelson M. & Guinea F. Gauge fields in graphene. *Phys. Rep.* **496**, 109-148 (2010).
- [10] Guinea F., Katsnelson M. I. & Geim A. K. Energy gaps and a zero-field quantum Hall effect in graphene by strain engineering. *Nature Phys.* **6**, 30-33 (2010).
- [11] Guinea F., Geim A. K., Katsnelson M. I. & Novoselov K. S. Generating quantizing pseudo-magnetic fields by bending graphene ribbons. *Phys. Rev. B* **81**, 035408 (2010).
- [12] Bahat-Treidel O., Peleg O., Grobman M., Shapira N., Segev M. & Pereg-Barnea T. Klein Tunneling in Deformed Honeycomb Lattices. *Phys. Rev. Lett.* **104**, 063901 (2010).
- [13] Juan F. de, Cortijo A., Vozmediano M. A. H. & Cano A. Aharonov-Bohm interferences from local deformations in graphene. *Nature Phys.* **7**, 810-815 (2011).
- [14] Verberck B., Partoens B., Peeters F. M. & Trauzettel B. Strain-induced band gaps in bilayer

- graphene. *Phys. Rev. B* **85**, 125403 (2012).
- [15] Tan, P. H., Han W. P., Zhao W. J., Wu Z. H., Chang K., Wang H., Wang Y. F., Bonini N. Marzari N., Pugno N., Savini G., Lombardo A. & Ferrari A. C. The shear mode of multilayer graphene. *Nature Mater.* **11**, 294-300 (2012).
- [16] Iyengar A., Wang J. H., Fertig H. A. & Brey L. Excitations from filled Landau levels in graphene. *Phys. Rev. B* **75**, 125430 (2007).
- [17] Lozovik Y. E. & Sokolik A. A. Electron-hole pair condensation in graphene bilayer. *Pis'ma v ZhETF* **87**, 61 (2008). [*JETP Lett.* **87**, 55 (2008)].
- [18] Berman O. L., Lozovik Y. E. & Gumbs G. Bose-Einstein condensation and superfluidity of magnetoexcitons in bilayer graphene. *Phys. Rev. B* **77**, 155433 (2008).
- [19] Berman O. L., Kezerashvili R. Ya. & Lozovik Y. E. Collective properties of magnetobiexcitons in quantum wells and graphene superlattices. *Phys. Rev. B* **78**, 035135 (2008).
- [20] Lozovik Y. E. & Yudson V. I. Generalization of Ginzburg-Landau equations for non-stationary problems in case of alloys with paramagnetic impurities. *Zh. Eksp. Teor. Fiz.* **71**, 738 (1976) [*Sov. Phys. JETP* **44**, 389 (1976)].
- [21] Snoke D. W. Spontaneous Bose Coherence of Excitons and Polaritons. *Science* **298**, 1368-1372 (2002).
- [22] Eisenstein J. P. & MacDonald A. H. Bose-Einstein condensation of excitons in bilayer electron systems. *Nature* **432**, 691-694 (2004).
- [23] Laughlin R. B. Excitons in the fractional quantum hall effect. *Physica B+C* **126**, 254 (1984).

## Acknowledgments

This work was supported by Natural Science Foundation of China under Grants No. 90921003, No. 10904005, and No. 11004013, and by the National Basic Research Program of China (973 Program) under Grant No. 2009CB929103.

**Author contributions** All authors equally contributed to this work.

**Competing financial interests** The authors declare no competing financial interests.

**Author Information** Correspondence and requests for materials should be addressed to P. Z. (zhang\_ping@iapcm.ac.cn).

## Supplementary Information

### Pseudo-magnetoexcitons in strained graphene bilayers without external magnetic fields

Zhigang Wang,<sup>1</sup> Zhen-Guo Fu,<sup>2,1</sup> Fawei Zheng,<sup>1</sup> and Ping Zhang<sup>1,3</sup>

<sup>1</sup>*LCP, Institute of Applied Physics and Computational Mathematics, P. O. Box 8009, Beijing 100088, China*

<sup>2</sup>*SKLSM, Institute of Semiconductors, CAS, P. O. Box 912, Beijing 100083, China*

<sup>3</sup>*Beijing Computational Science Research Center, Beijing 100089, China*

**I.** Let us explain first how to derive the Hamiltonian (2) of the main text. Taking the coordinate transformations

$$\mathbf{P}=2\frac{l_e\mathbf{p}^e+l_h\mathbf{p}^h}{l_e+l_h}, \mathbf{p}=\frac{l_e\mathbf{p}^e-l_h\mathbf{p}^h}{l_e+l_h}, \quad (\text{S1})$$

$$\mathbf{R}=\frac{l_h\mathbf{r}^e+l_e\mathbf{r}^h}{l_e+l_h}, \mathbf{r}=2\frac{l_h\mathbf{r}^e-l_e\mathbf{r}^h}{l_e+l_h}, \quad (\text{S2})$$

we can rewrite  $h_0^{e/h}$  in Eq. (1) as

$$h_0^{e/h}=\left\{\kappa_{e/h}\left(\frac{P_x}{2}\pm p_x\right)+i\left[\left(\frac{P_y}{2}\pm p_y\right)\mp\xi\left(X\pm\frac{x}{2}\right)\right]\right\}, \quad (\text{S3})$$

where  $\kappa_{e/h}=(l_e+l_h)/(2l_{e/h})$ , and  $\xi=1/(2l_e l_h)$ . Here,  $\gamma=l_e/l_h=\sqrt{B_s^h/B_s^e}$  describes the inhomogeneity of PMFs suffered by electrons and holes in different layers. In the limit of  $\gamma=1$ , the problem of PME in SGB is reduced to that of PME in a uniform PMF, which are consistent with those on the magnetoexcitons in an external magnetic field [1, 2]. And then one can introduce the transformation  $S=e^{iXy/l_e l_h}$ , for which  $S^\dagger P_x S=P_x+y/l_e l_h$ ,  $S^\dagger p_y S=p_y+X/l_e l_h$ , and shift  $\mathbf{r}\rightarrow\mathbf{r}-l_e l_h \hat{\mathbf{z}}\times\mathbf{P}$ ,  $h_0^{e/h}$  can be further written as

$$h_0^{e/h}=\kappa_{e/h}\{(\pm p_x+\xi y)\pm i(p_y\mp\xi x)\}. \quad (\text{S4})$$

The relative coordinate of electron and hole in the  $x$ - $y$  plane  $\mathbf{r}^e-\mathbf{r}^h$  becomes  $\tilde{\mathbf{r}}=\frac{1}{2}(\gamma-\gamma^{-1})\mathbf{R}+\frac{1}{4}(2+\gamma+\gamma^{-1})(\mathbf{r}-l_e l_h \hat{\mathbf{z}}\times\mathbf{P})$ . Finally we define the harmonic lowering operators

$$a=\sqrt{l_e l_h}p_x-i\frac{x}{2\sqrt{l_e l_h}}, b=\sqrt{l_e l_h}p_y-i\frac{y}{2\sqrt{l_e l_h}}, \quad (\text{S5})$$

and their combination

$$c_\pm=\pm(a\pm ib)/\sqrt{2}. \quad (\text{S6})$$

Substituting them into Eq. (1), we can obtain the Hamiltonian (2) of the main text. The eigenvalues, i.e., the PLLs of  $H_0$  without CI are given by Eq. (3) and the corresponding eigenvectors are given by

$$|n_+, n_-\rangle_0 = 2^\eta \begin{pmatrix} s_+ s_- \Phi_{|n_+|-1, |n_-|-1}(\mathbf{r}) \\ s_- \Phi_{|n_+|, |n_-|-1}(\mathbf{r}) \\ s_+ \Phi_{|n_+|-1, |n_-|}(\mathbf{r}) \\ \Phi_{|n_+|, |n_-|}(\mathbf{r}) \end{pmatrix}, \quad (\text{S7})$$

where  $\eta = \frac{\delta_{n_+,0} + \delta_{n_-,0} - 2}{2}$ ,  $s_\pm = \text{sgn}(n_\pm)$ , and  $\Phi_{n_1, n_2}(\mathbf{r}) = \frac{2^{-\frac{|l_z|}{2}} n_\pm! e^{-il_z \phi} \delta(l_z) r^{|l_z|}}{\sqrt{2\pi n_1! n_2!}} L_{n_-}^{|l_z|}(\frac{r^2}{2}) e^{-\frac{r^2}{4}}$  with  $l_z = n_1 - n_2$ ,  $n_- = \min(n_1, n_2)$ ,  $\delta(l_z) = \text{sgn}(l_z)^{l_z} \rightarrow 1$  for  $l_z = 0$ , and  $L(x)$  the Laguerre polynomial. To obtain eigenvalues of the total Hamiltonian  $H$ , we need to solve the following equation:

$$0 = \det \left\| \delta_{n_+, n'_+} \delta_{n_-, n'_-} (E_{n_+, n_-}^{(0)} - E) \right. \\ \left. + {}_0\langle n'_+, n'_- | U(\tilde{\mathbf{r}}) | n_+, n_- \rangle_0 \right\|. \quad (\text{S8})$$

Here, the intra-PLL component of the CI is defined as  ${}_0\langle n_+, n_- | U | n_+, n_- \rangle_0$ , while the inter-PLL component is defined as  ${}_0\langle n'_+, n'_- | U | n_+, n_- \rangle_0$ , where  $|n'_+, n'_-\rangle_0 \neq |n_+, n_-\rangle_0$ . The PLLs as a function of  $R$  are presented in supplementary Figure S1.

**II.** From the Fermi's golden rule, the optical absorption for photons of frequency  $\omega$  yields

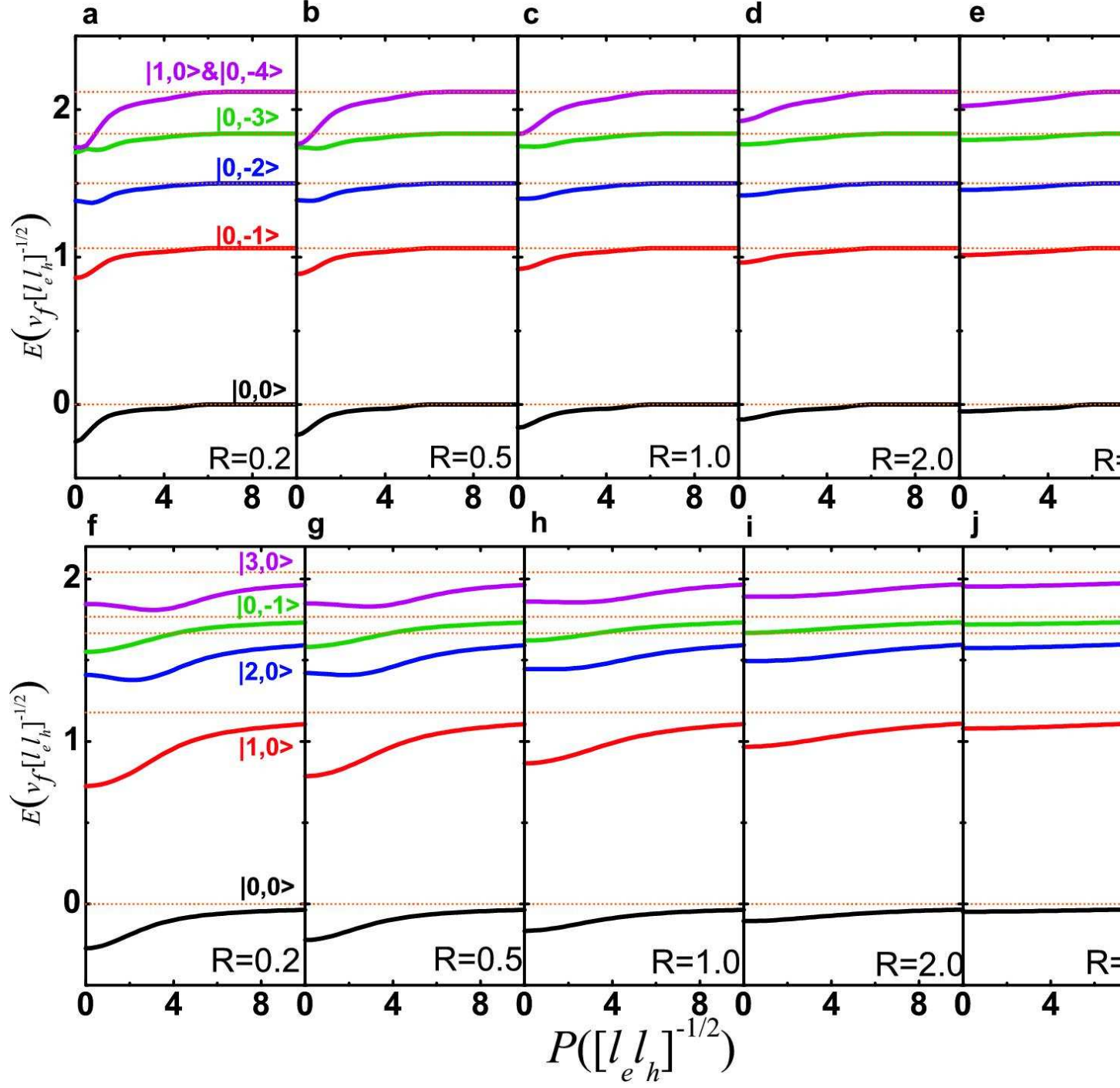
$$R_{ab}(R, \omega) = \frac{2\pi}{\hbar} \sum_{\alpha} \left| \langle \alpha | \frac{e}{c} \mathbf{A} \cdot \mathbf{v} | 0 \rangle \right|^2 \delta(\varepsilon_{eh}^{(\alpha)}(R) - \varepsilon_0 - \hbar\omega), \quad (\text{S9})$$

where  $|\alpha\rangle$  is the set of quantum numbers describing a particle-hole excitation and  $|0\rangle \equiv |\mu, \mu\rangle$  is the ground state in absence of particle-hole excitations with  $\varepsilon_0$  being the corresponding ground state energy.  $\mathbf{v} = \partial H_0 / \hbar \partial \mathbf{p}$  is the velocity operator for free part of Hamiltonian, and  $\mathbf{A}$  is the vector potential. For linear polarized light  $\mathbf{A} = A \hat{\mathbf{x}}$ , choosing a Lorentzian type broadening, one has

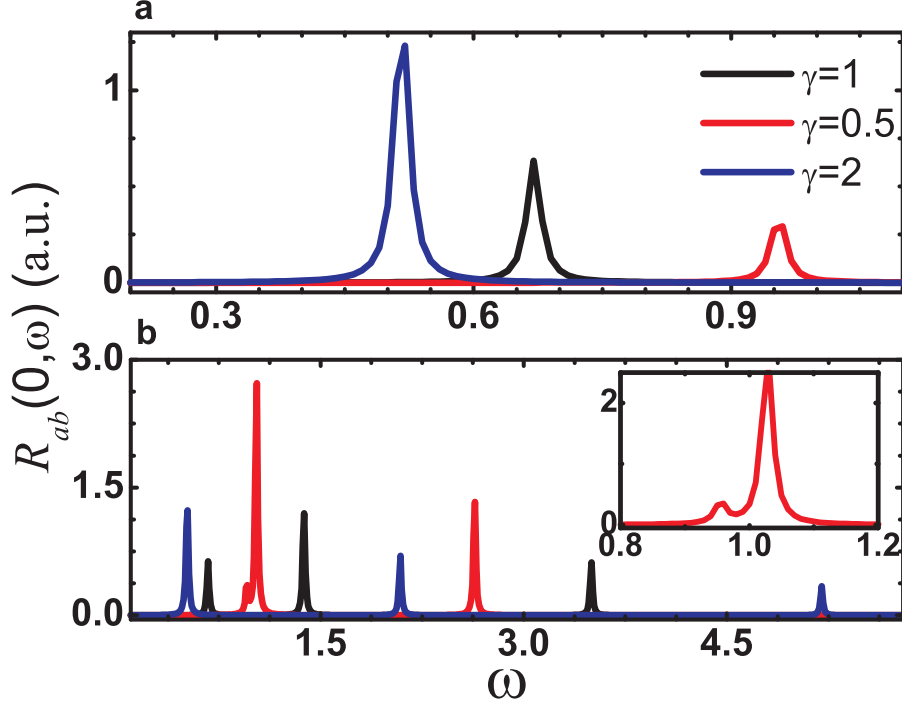
$$R_{ab}(R, \omega) \propto \sum_{\alpha} |\langle \alpha | v_x | 0 \rangle|^2 \frac{\Gamma/2}{(\varepsilon_{eh}^{(\alpha)}(R) - \varepsilon_0 - \hbar\omega)^2 + \Gamma^2/4}, \quad (\text{S10})$$

where  $\Gamma$  denotes the linewidth, and  $|\langle \alpha | v_x | 0 \rangle|^2 = \sum_{n_+ > \mu} \sum_{n_- \leq \mu} \int T d\mathbf{r}$  is for full occupation while  $\sum_{n_+ \geq \mu} \sum_{n_- \leq \mu} \int T d\mathbf{r}$  is for partial occupation. The parameter  $T$  is defined as

$$T = |C_{n_+, n_-}^\alpha \langle n_+, n_- | v_x | \mu, \mu \rangle|^2, \quad (\text{S11})$$



Supplementary Figure S1: Dispersions of the first few PLLs as functions of  $P$  with different  $R$ . The imbalance parameter  $\gamma=0.5$  for **a-e** while  $\gamma=1.5$  for **f-j**, and other parameters are same as Figure 2 in main text.



Supplementary Figure S2: **The optical absorption curves of PMEs with  $\mu=1$ .** **a**, Fully and **b** partially occupied cases as functions of photon energy  $\omega$  ( $\hbar=1$ ). The spacer thickness is set to  $d=0.2$ .  $\beta=0.49$ . The inset in **b** is the enlarged dispersion curves between  $\omega=0.8$  and  $\omega=1.2$ .

where  $C_{n_+, n_-}^\alpha$  is the projection of PME state  $|\alpha\rangle$  on the basis state  $|n_+, n_- \rangle$ . In the absence of inter-PLL CI which is much weaker than intra-PLL CI, the PME state  $|\alpha\rangle$  is one special basis state and  $C_{n_+, n_-}^\alpha = \delta_{\alpha, (n_+, n_-)}$ , same as that in the noninteracting case. As a result, we can analytically obtain the optical absorption selection rule for PMEs, Eq. (4) in main text.

As an example, we additionally plot the optical absorption spectrum with  $\mu=1$  fully and partially occupied cases in supplementary Figure S2. The selection rule for fully occupied case with  $\mu=1$  promises that there is only one resonant peak to occur, which corresponds to the formation of PME state  $|2, 1\rangle$  by absorbing a photon quanta  $\hbar\omega$ . For partially occupied case, however, there are three non-zero elements according to selection rule (4), which are  $|1, 0\rangle$ ,  $|1, -2\rangle$ , and  $|2, 1\rangle$ . Therefore, there are three resonant peaks appearing in optical absorption spectrum, see supplementary Figure S2b. Similar to those in Fig. 3 in main text for the  $\mu=0$  cases, the imbalance of strain-induced PMFs changes the location of the resonant peak. When the imbalance parameter  $\gamma \neq 1$ , these resonant peak moves in a more complex way.

**III.** In the limit of  $d \rightarrow \infty$  and  $B_s \rightarrow \infty$ , the PME energy can be approximated by only considering its zeroth order energy part  $E_{n,m}^{(0)}$ . However, if the PMF is about 10~20T, CI can be treated as a perturbation since CI  $e^2/\epsilon d$  is just several times less than  $\hbar v_f/\sqrt{l_e l_h}$ . In the absence of inter-PLL CI, by substituting the approximate relation [3]

$$\langle \langle nmP | U(\tilde{\mathbf{r}}) | nmP \rangle \rangle = \varepsilon_{nm}^{(b)} + \frac{P^2}{2M_{mn}(B_s, d)} \quad (\text{S12})$$

for  $R=0$  into Eq. (S8), we can get the asymptotic dispersion law of a PME for small magnetic momenta. Here the notation  $\langle \langle nmP | U(\tilde{\mathbf{r}}) | nmP \rangle \rangle$  denotes the averaging by the two-dimensional harmonic oscillator eigenfunctions  $\Phi_{n,m}(\mathbf{r})$ , and  $\varepsilon_{nm}^{(b)}$  is the binding energy, and finally one can obtain the Eqs. (6) and (7) in main text.

- 
- [1] Iyengar A., Wang J. H., Fertig H. A. & Brey L. Excitations from filled Landau levels in graphene. *Phys. Rev. B* **75**, 125430 (2007).
  - [2] Wang Z., Fu Z.-G. & Zhang P. Magnetoexcitons and optical absorption of bilayer-structured topological insulators. *Appl. Phys. Lett.* **100**, 161602 (2012).
  - [3] Berman O. L., Lozovik Y. E. & Gumbs G. Bose-Einstein condensation and superfluidity of magnetoexcitons in bilayer graphene. *Phys. Rev. B* **77**, 155433 (2008).